Numerical Investigation on Thermo-Hydraulic Enhancement of Compact Plate Heat Exchangers Using Bionic Patterns

Karthik TH[1], Nitish S[2], P Ajay[3], Varshith G[4], Jyothi Prakash K H *[5]

[1,2,3,4] *Student, Department of Mechanical Engineering. PES University, Bangalore, Karnataka, India*

[*5] *Assistant Professor, Department of Mechanical Engineering. PES University, Bangalore, Karnataka, India*

Abstract

This study presents a novel approach to enhancing the thermo-hydraulic performance of compact Brazed Plate Heat Exchangers (BPHE) through the application of bionic patterns. Specifically, we developed snowflake and wishbone winglet patterns inspired by natural formations to optimize the heat transfer rate and reduce pressure loss. The snowflake pattern, characterized by its six-fold rotational symmetry, and the wishbone pattern, featuring an innovative cavity design, were fabricated using advanced additive manufacturing techniques. Computational Fluid Dynamics (CFD) simulations were conducted using Ansys Fluent 19.2 to analyze the performance under various operating conditions, with temperatures ranging from 90°C to 40°C and mass flow rates between 0.01 kg/s and 0.05 kg/s. The simulation results were validated against experimental data. The findings demonstrate that the snowflake and wishbone patterned BPHEs achieve pressure losses that are 36% and 80% lower, respectively, compared to traditional chevron-type BPHEs. Moreover, the heat transfer rates for these novel patterns improved by 22.5% and 28.7%, respectively. These results underscore the potential of bionic designs in significantly enhancing BPHE performance.

Keywords: *Heat Exchanger, Effectiveness, Heat transfer Coefficient, Bionic pattern*

NOMENCLATURE:

Q	Heat transfer rate(W)
m	Mass flow rate (kg/s)
T_i	Inlet temperature (K)
T_o	Outlet temperature (K)
ΔT	Temperature difference (K)
k_{walls}	Thermal Conductivity of walls (W/m-K)
r_{walls}	Thermal Resistance of walls (m^2-K/W)
$h_{w,c}$	HTC of cold fluid (W/m^2-K)
$h_{w,h}$	HTC of hot fluid (W/m^2-K)
ΔP	Pressure drop (Pa)
U	Overall heat transfer coefficient (W/m^2-K)
c	Specific Heat Capacity (J/kg-K)
E	Energy per unit mass (J/kg)
C	Heat capacity (W/K)
ρ	Density (kg/m^3)
t	Time
p	Pressure (Pa)
τ_{ij}	Components of the Stress tensor (Pa)
g	Acceleration due to gravity (m/s^2)
μ	Laminar viscosity (kg/m-s)
μ_t	Turbulent viscosity (kg/m-s)

Non-Dimensional numbers:

Re	Reynolds Number
ε	Effectiveness
Pr	Prandtl number

Subscripts:

c	Cold fluid
h	Hot fluid
w	Water

Abbreviations:

HTC	Heat Transfer Coefficient (W/m^2-K)
CFD	Computational Fluid Dynamics
BPHE	Brazed Plate Heat Exchanger
PHE	Plate Heat Exchanger
HX	Heat Exchanger

1.Introduction

Heat exchangers are designed to effectively transfer heat between two different media. Heat exchangers find extensive use in power plants, refrigeration, air conditioning and heating systems, vehicle cooling systems, and several other engineering applications. They are particularly effective in situations where there is a high temperature difference between the two fluids. Heat exchangers come in a variety of designs, each design has its own advantages and limitations, and the choice of design depends on various factors, such as the type of fluids being used, their flow rates and temperatures, and the required heat transfer rate. PHE are designed with thin, parallel metal plates for optimal heat exchange. Among PHEs, brazed plate heat exchangers (BPHEs) stand out for their compactness and durability. BPHEs feature corrugated plates brazed together, forming leak-tight channels for fluid flow. They excel in heating, cooling, and refrigeration systems due to their efficiency and reliability.

The performance of a PHE is dependent on the pattern of the plates. The common patterns are chevron or herringbone pattern. Kim and Park [1] experimented on BPHE with different chevron geometry and hydraulic diameter, and it was found that the compact BPHE has high pressure loss but it also improves heat transfer rate. Kwon et al. [2] have conducted experiment on PHE using refrigerant R-1233zd(E) and water. In the experiment of single-phase water to water, HTC correlation was obtained using Wilson plot. Similar research was performed by Mutumba et al. [3] where they also used Wilson plot technique to find the correlation for HTC. Soman et al. [4] conducted an experiment on dimple type PHE using nanofluid γ-Al_2O_3 and found that γ-Al_2O_3 had better heat transfer properties than water. Soman et al. [5] have also performed CFD simulation on the same dimple plate heat exchanger of [4]. It was found the that deviation between experimental results and CFD simulation was ± 20%. The deviation could be due to heat losses in the experimental system whereas CFD simulation was performed in adiabatic conditions. Aradag et al. [6] have performed CFD simulation on gasketed PHE and validated it against experimental results, it was found that experimental results and CFD results have a mean deviation of about 10%. Yoon et al. [7] have conducted numerical analysis on PHE using a flow network approach. It found that the experimental and CFD results have a mean deviation of 10%. Luan et al. [8] have also performed a simulation for a welded PHE, it was seen that the influence of mesh quality could impact the results of CD simulation. The CFD simulation results deviated from experimental results with a mean deviation of about 15%.

Since CFD results have maximum deviation of 15% from experimental results, the study of plate heat exchanger using CFD simulation could be considered for further studies. Pourhoseinian et al. [9] have performed CFD simulation on a membrane plate heat exchanger. Simulation tests were conducted on both single and multi-flow channels, revealing that the multi-flow channel exhibits superior thermal performance compared to the single

flow channel. Xu et al. [10] conducted a CFD simulation on a Plate and fin heat exchanger. The simulation was performed for various geometric parameters of a fin. It was found that overall performance can be increased by decreasing fin thickness and increasing fin spacing. Kobayashi et al. [11] performed topology optimization on HX. It is found that the heat exchanger thermal performance was increased with moderate pressure loss, similar kind of study was performed by Liu et al. [12].

Djemel et al. [13] have performed CFD simulation on an intercooler with a Y-shape bionic pattern inspired by the bronchiole of the respiratory system. It was found that Y-shape bionic increased the thermal effectiveness by 97.66%. Goltas et al. [14] have performed CFD simulation on PHE with fish gills as corrugation pattern, it was found that fish gills pattern enhanced heat transfer by 17.5% when compared with chevron types PHE. Gürel et al. [15] performed a CFD simulation on PHE which has lung pattern embossed on a plate. It was found that lung pattern reduces pressure loss by 67.8% and enhances heat transfer rate by 71.3% when compared with reference PHE. Eldeeb et al. [16] performed CFD simulation on pillow type PHE and found that it increases HTC by 38% and reduces pressure drop by 72% when compared with chevron type PHE

From the extensive literature survey, it is seen that much of the research work to improve the heat transfer performance in the PHE focused solely on the Herringbone pattern, also known as Chevron. However, the survey also explored the possibility of enhancement in the heat transfer in plate exchanger with the use of bionic patterns. Hence in the present study the objective is to design a plate heat exchanger incorporating two distinct corrugation patterns namely Snowflake and Wishbone patterns and investigate their effects on the plate heat exchanger performance. The bionic pattern proposed in the present work was inspired by Snowflakes formed in clouds when the temperature falls below freezing point and Wishbone found in the birds. It is known that the Snowflake pattern has six sided and six folded rotational symmetry as shown in Fig.2. Snowflake structure can enhance heat transfer process as it is typically formed by liquid to solid phase change in nature [17]. The wishbone pattern, inspired by avian anatomy, introduces a cavity structure that enhances fluid turbulence and mixing, thereby increasing heat transfer rates. The adoption of these bionic patterns, facilitated by advancements in additive manufacturing, not only improves heat transfer efficiency but also significantly reduces pressure drop, addressing a key limitation of conventional designs.

2.Methodolgy

2.1 Geometry Modelling

In this study, the effect of snowflake-patterned and wishbone-patterned PHE on pressure drop and heat transfer is investigated. The heat exchanger consists of 3 plates as shown in figure 1 over which the snowflake pattern and wishbone pattern are embedded and geometric details of the plate are given in Table 1. For the snowflake-patterned plate, two snowflakes are embedded on the plate symmetrically as shown in Fig. 2, similarly for the wishbone-patterned plate, 5 x 17 wishbone patterns are embedded on the plate as shown in Fig. 3.

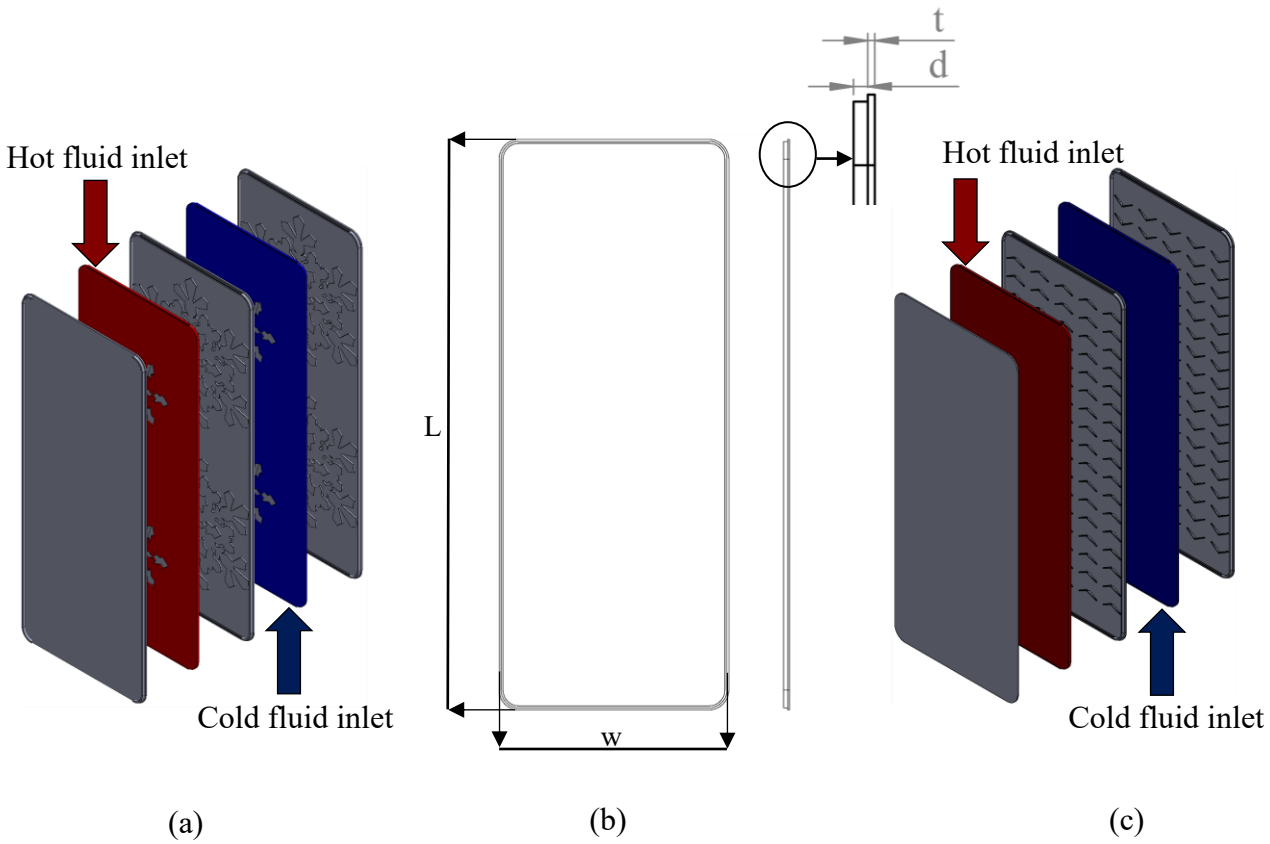

Fig. 1. (a) Stacked arrangement of Snowflake-patterned PHE, (b) Schematic diagram of PHE, (c) Stacked arrangement of Wishbone-patterned PHE

Table 1 Design Specification

Design Parameters	**Dimensions**
Plate thickness, t (mm)	1
Length, L (in mm)	287
Width, w (in mm)	117
Spacing Between the plates, d (mm)	2
Plate material	Stainless steel 316

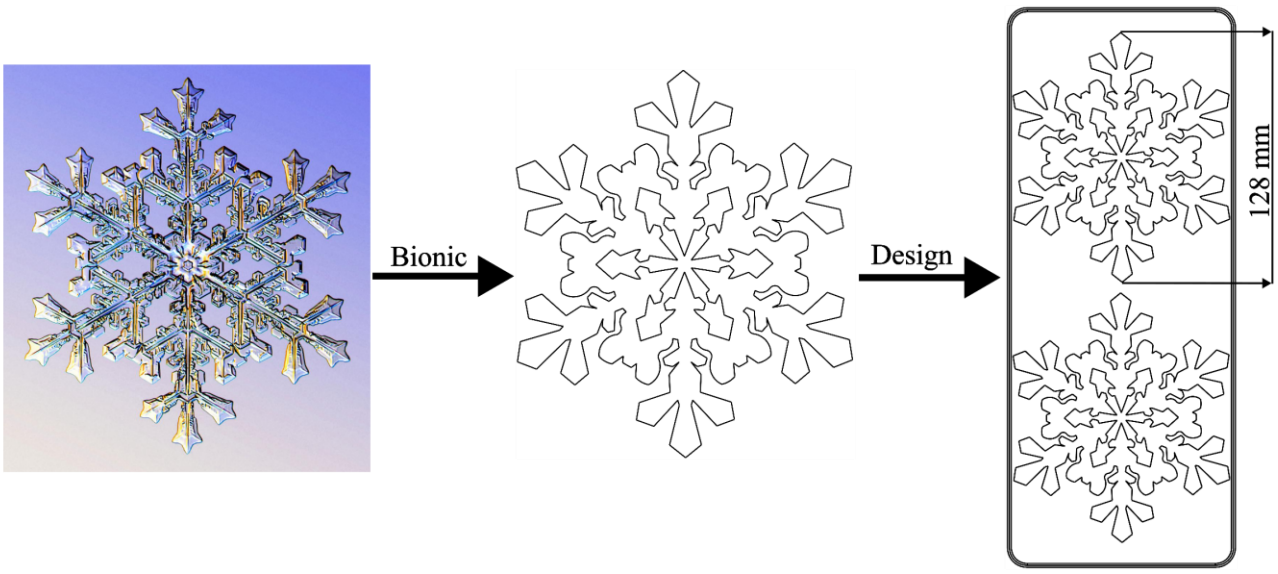

Fig. 2. Schematic illustration depicting the Snowflake-patterned PHE

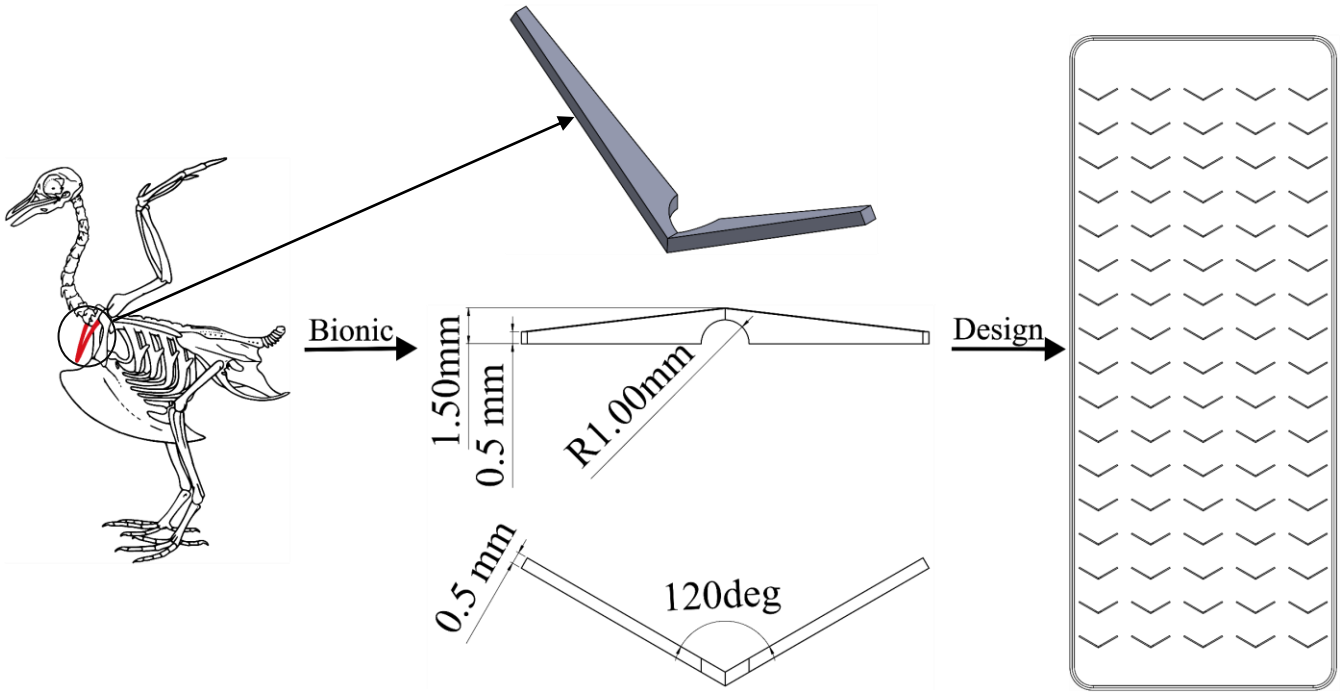

Fig. 3. Schematic illustration depicting of Wishbone-patterned PHE

2.2 Meshing and Grid Independence

Meshing is a pivotal aspect of Computational Fluid Dynamics research, involving the division of the simulation domain into smaller elements. This process is essential for accurately modeling fluid flow, influencing the reliability and precision of research findings. The solid model is meshed with a Face sizing of 0.5mm initially using Ansys Fluent meshing and the type of element used for discretization is Polyhexcore. The meshing was refined around a corrugated pattern. Figure 4 and 5 show the discretization of the plate using fluent meshing. The number of mesh elements formed using this value was 3,595,557 for snowflake-patterned PHE and 2,984,536 for wishbone-patterned PHE. Grid independence is a common practice in numerical simulations and computational modeling. It refers to the process of verifying that the results of a simulation are not significantly affected by the size or density of the mesh used to discretize the simulation domain. Table 2 and Table 3 provides the details for grid independence study, from the table, results between 35 lakhs and 102 lakhs mesh elements are almost constant for snowflake-patterned PHE, and similarly, the results between 29 lakhs and 92 lakhs mesh elements are almost constant for wishbone-patterned PHE. For this reason, 35 and 29 lakh mesh elements are used in the further study for snowflake-patterned and wishbone-patterned respectively.

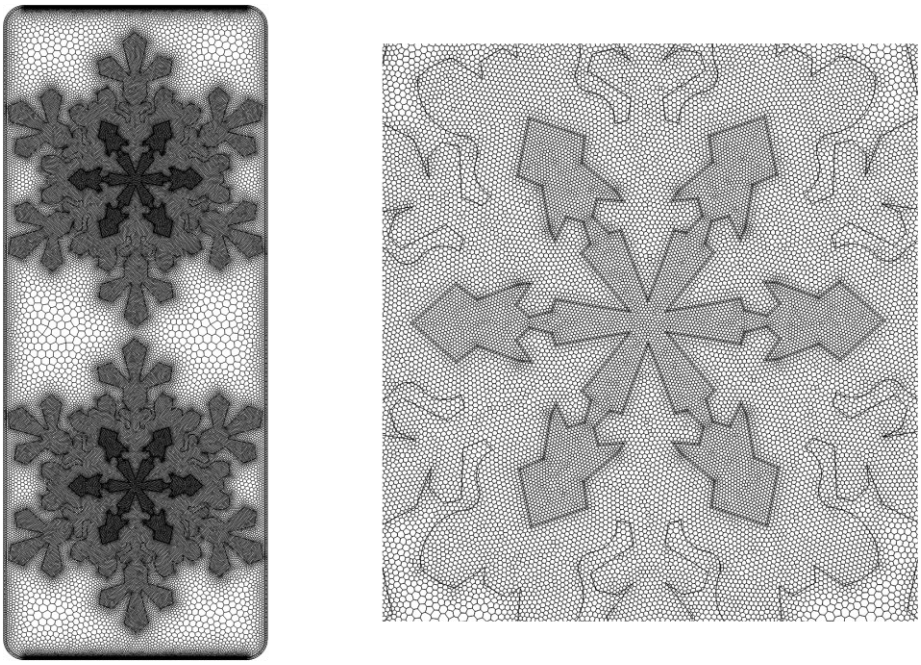

Fig. 4. Discretization of Snowflake-patterned PHE

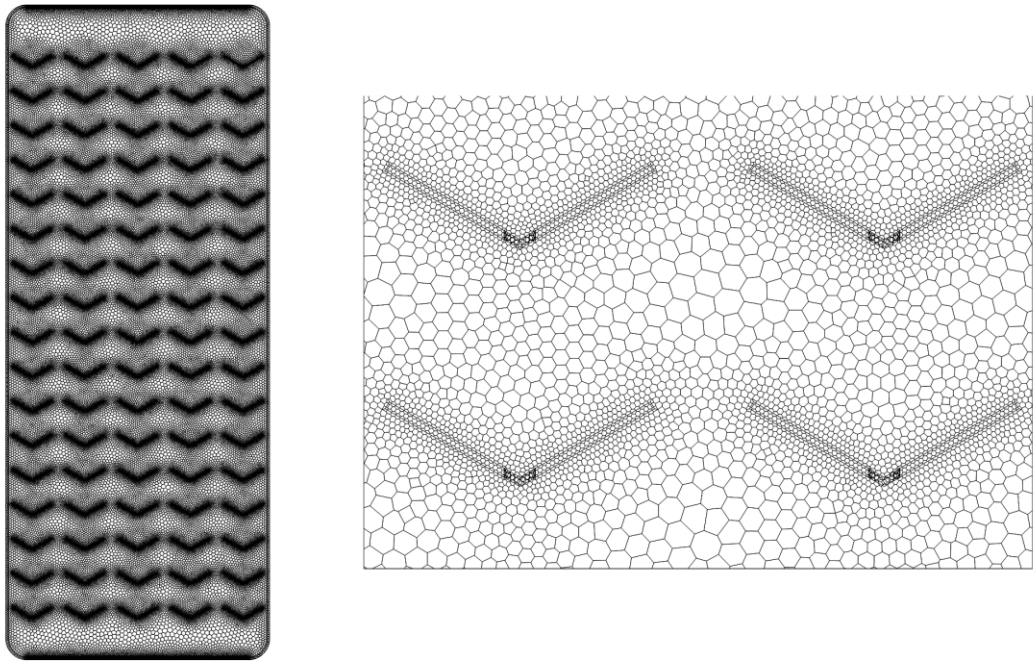

Fig. 5. Discretization of Wishbone-patterned PHE

Table 2 Grid independence study for Snowflake-patterned PHE

Number of mesh elements	T_{ho} (ºC)	T_{co}(ºC)	Pressure drop (Pa)
3527364	72.50	56.44	1434.33
4387693	72.42	56.35	1430.27
5649247	72.56	56.47	1434.67
7386492	72.52	56.44	1434.42
8847126	72.54	56.49	1434.59
10255489	72.57	56.51	1434.94

Table 3 Grid independence study for Wishbone-patterned PHE

Number of mesh elements	T_{ho} (ºC)	T_{co}(ºC)	Pressure drop (Pa)
2974566	72.37	56.85	638.75
3648596	72.35	56.81	637.91
4521783	72.36	56.84	638.40
5874632	72.34	56.83	638.57
7324691	72.37	56.87	638.72
9245811	72.39	56.91	638.67

2.3 Governing Equation and Turbulence Modelling

To determine the characteristics of the flow field, it's necessary to solve the conservation equations for energy, momentum and mass. Continuity equation ensures mass conservation which is given by Equation (1), the Navier-Stokes equation addresses momentum dynamics which is given by Equation (2), and the energy equation governs heat transfer rate which is given by Equation (3)

$$\frac{\partial \rho}{\partial t} + \frac{\partial}{\partial x_i}\left(\rho u_i\right) = 0 \tag{1}$$

$$\frac{\partial \left(\rho u_i\right)}{\partial t} + \frac{\partial}{\partial x_j}\left(\rho u_i u_j\right) = -\frac{\partial p}{\partial x_i} + \frac{\partial \tau_{ij}}{\partial x_j} + \rho g_i \tag{2}$$

$$\frac{\partial \left(\rho E\right)}{\partial t} + \frac{\partial}{\partial x_i}\left(\rho E u_i\right) = \frac{\partial}{\partial x_i}\left(k\frac{\partial T}{\partial x_i}\right) + \rho u_i g_i + Q \tag{3}$$

The turbulence model used are two-equation models, two-equation models are a category of Reynolds-averaged Navier–Stokes (RANS) models that aim to provide closure for the turbulent stresses in the Reynolds-averaged equations. RNG k-epsilon has better near wall treatment even without explicitly modeling boundary layers and hence improves accuracy. Transport Equations for RNG k-ε is shown in Equation (4) and (5).

Turbulence Kinetic Energy:

$$\frac{\partial}{\partial t}\left(\rho k\right) + \frac{\partial}{\partial x_i}\left(\rho k u_i\right) = \frac{\partial}{\partial x_j}\left[\left(\mu + \frac{\mu_t}{\sigma_k}\right)\frac{\partial k}{\partial x_j}\right] + P_k - \rho\varepsilon \tag{4}$$

Specific Dissipation Rate:

$$\frac{\partial}{\partial t}\left(\rho \varepsilon\right) + \frac{\partial}{\partial x_i}\left(\rho \varepsilon u_i\right) = \frac{\partial}{\partial x_j}\left[\left(\mu + \frac{\mu_t}{\sigma_\varepsilon}\right)\frac{\partial \varepsilon}{\partial x_j}\right] + C_{1\varepsilon}\frac{\varepsilon}{k}P_k - C_{2\varepsilon}^{*}\rho\frac{\varepsilon^2}{k} \tag{5}$$

For the analysis, RNG k-ε turbulence model and second order upwind solution method are used. CFD Simulation was performed in Ansys Fluent, with water as a working fluid. Table 4 provides details regarding the selected simulation model, while Table 5 outlines the operating conditions utilized for the present study.

Table 4 Parameters Set for CFD Simulation

Solver Type	Pressure-based
Turbulence model	RNG k-ε turbulence model
Solver Method	Second Order method
Velocity-Pressure interaction	SIMPLE

Table 5 Operating Condition

Fluid	Mass flow rate (kg/s)	T_i (^{0}C)
Hot	0.01-0.05	90
Cold	0.01-0.05	40

The temperature difference between outlet and inlet of cold fluid is given by:

$$\Delta T_c = T_{co} - T_{ci} \tag{6}$$

The temperature difference between outlet and inlet of hot fluid is given by:

$$\Delta T_h = T_{hi} - T_{ho} \tag{7}$$

The heat transfer rate for cold fluid and hot fluid has been calculated using the temperature difference as follows:

$$Q_c = m_c c_p \Delta T_c \tag{8}$$

$$Q_h = m_h c_p \Delta T_h \tag{9}$$

The effectiveness of HX is given by:

$$\varepsilon = \frac{Q_{actual}}{Q_{\max}} \tag{10}$$

In order to obtain effectiveness, the maximum rate of heat transfer and actual rate of heat transfer is given by:

$$Q_{\max} = C_{\min} \Delta T \tag{11}$$

$$Q_{actual} = m_h c_p \Delta T_h = m_c c_p \Delta T_c \tag{12}$$

To find maximum rate of heat transfer, the temperature difference and minimum heat capacity is given by:

$$\Delta T = T_{hi} - T_{ci} \tag{13}$$

$$\begin{aligned} C_{\min} &= m_h c_h, if\ \ m_h c_h < m_c c_c \\ C_{\min} &= m_c c_c, if\ \ m_c c_c < m_h c_h \end{aligned} \tag{14}$$

2.4 Data Reduction

Local HTC has been calculated using the data obtained from Fluent. These data values have been obtained along the surface of the plate. Local HTC, h_x is calculated by using the wall temperature and fluid temperature which is given by equation (15). The calculation of the average HTC is performed through Equation (16). Due to the extensive dataset, MATLAB was employed to compute the average HTC.

Local Heat Transfer Coefficient:

$$h_x = \frac{q_x}{T_f - T_w} \tag{15}$$

Where, T_w is the wall temperature, T_f is fluid temperature and q_x is local heat flux.

Average Heat Transfer Coefficient:

$$h_{avg} = \frac{1}{A}\iint h_x dA \tag{16}$$

Reynolds Number:

$$\mathrm{Re} = \frac{\rho V D_h}{\mu} \tag{17}$$

Hydraulic Diameter:

$$D_h = \frac{4 * A}{P} \tag{18}$$

3.Validation

To verify the methodology outlined in Section 2, we compared the estimated results with experimental data. Specifically, we compared the numerical analysis conducted in Ansys Fluent [18] with the experimental findings of Kwon et al [2] for a brazed PHE with grooves featuring Chevron angles on the plates. The validation focused on a scheme of a brazed PHE with corrugated characteristics, as depicted in Figure 6. The geometric attributes of the PHE from [2] are detailed in Table 6 for comparison, while Table 7 outlines the various cases examined for different mass flow rates and their corresponding temperatures for the hot and cold fluids. This validation process specifically targeted the single-phase water-to-water experiment. Simulations were conducted using approximately 102 lakhs Polyhexcore mesh elements.

Table 6 Design Specification	
Design Parameters	**Dimensions**
Chevron angle (degrees)	60
Enlargement factor	1.15
Hydraulic diameter [mm]	3.32
Wavelength [mm]	7.5
Length of flow [mm]	234
Thickness of the Plate [mm]	0.4
Width of plate [mm]	117
Pitch [mm]	1.94
Plate material	Stainless steel 316

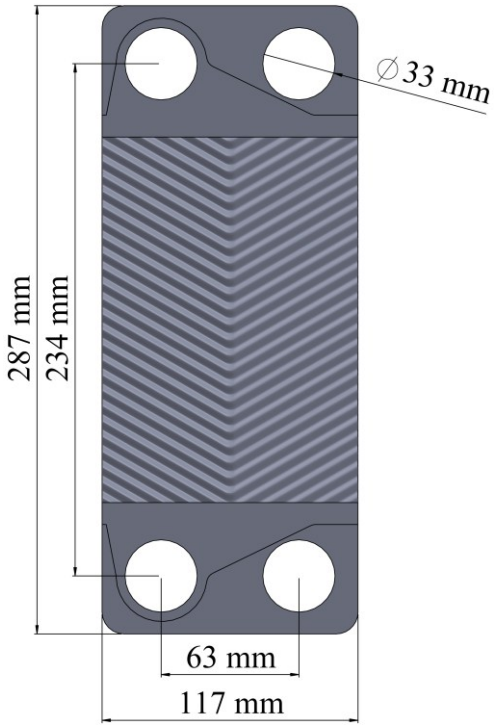

Fig. 6. Illustration depicting the Plate Heat Exchange

Table 7 Boundary Conditions

Case:	fluid	Temperature (K)	mass flow rate (kg/s)
1	Hot	310.85	0.0412
	Cold	302.75	0.0788
2	Hot	317.85	0.0412
	Cold	310.15	0.0740
3	Hot	323.85	0.0412
	Cold	315.15	0.0675

After performing CFD simulation, the obtained results are compared with experimental results [2] and shown in Table 8. The CFD simulation yielded results with a maximum error of 6.25%, indicating good numerical model accuracy. This suggests the model is suitable for further studies or analysis. Validation against real-world data and sensitivity analysis can enhance confidence in the model.

Table 8. Comparison of CFD and Experimental Results

Case:	T_{hi} (^{0}C)	T_{ci}(^{0}C)	$U_{experimental}$ (W/m^{2}K)	U_{cfd} (W/m^{2}K)	% error
Case 1	37.7	29.6	2673.916	2506.776	6.25
Case 2	44.7	37	2711.748	2824.218	4.147
Case 3	50.7	42	2716.468	2879.567	6.004

4.Results and Discussion

In this study, CFD simulations are conducted to evaluate pressure drop and rate of heat transfer of a PHE with Snowflake and Wishbone Pattern. This methodology is validated against the experimental results of Kwon et al [2]. The CFD simulation was performed for the operating conditions as mentioned in section 2.3.

4.1 Effect of Re on ΔT:

The mass flow rates of the cold and hot fluids are varied from 0.01 kg/s to 0.05 kg/s in 0.01 kg/s increments, resulting in Reynolds numbers ranging from 193 to 966 for the cold fluid and 397 to 1985 for the hot fluid. The inlet temperatures are set at 40°C for the cold fluid and 90°C for the hot fluid. ΔT_c and ΔT_h is calculated using Equation (6) and (8). Figure 7(a) and 7(b) illustrate the relationship between ΔT_h and the varying Reynolds number of the hot fluid. It is observed that ΔT_h decreases as the Reynolds number increases, indicating a transition to turbulent flow. This transition enhances the mixing of the hot fluid, resulting in a thinner thermal boundary layer and more efficient heat transfer to the cold fluid. As the Reynolds number of the cold fluid increases, it also transitions to turbulent flow, contributing to an increase in ΔT_h. A significant rise in ΔT_h by 35% to 80% for snowflake-patterned PHE and 39% to 77% for wishbone-patterned PHE is evident as the Reynolds number of the cold fluid increases from 193 to 966.

Correspondingly same characteristics are observed for ΔT_c as seen in Figure 8(a) and 8(b). It is observed that there is a significant rise in ΔT_c 41% to 93% for snowflake-patterned PHE and 41% to 82% for wishbone-patterned PHE as the Reynolds number of the hot fluid increases from 397 to 1985. Therefore, turbulent flow in both fluids emerges as a key factor for improving heat transfer in the system.

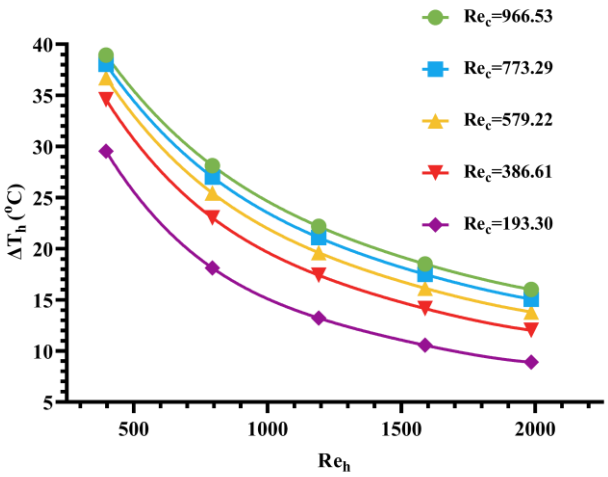

(a)

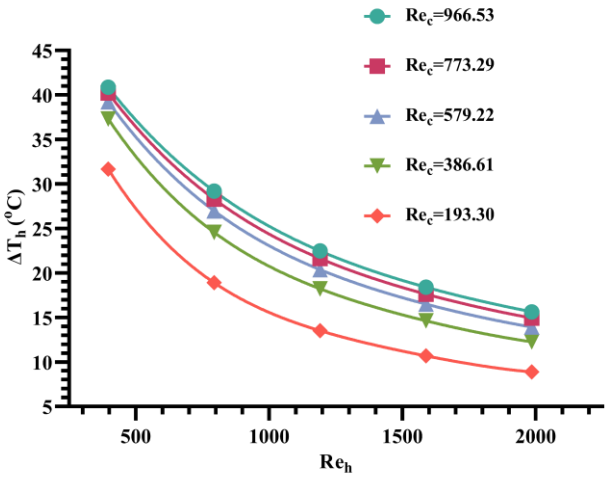

(b)

Fig. 7. Plot of ΔT_h vs Reynolds number of the hot fluid across a range of Reynolds numbers of cold fluid for (a) Snowflake-patterned PHE and (b)wishbone-patterned PHE

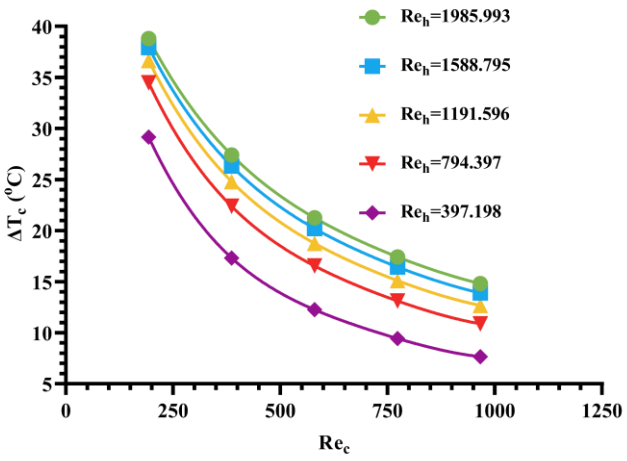

(a)

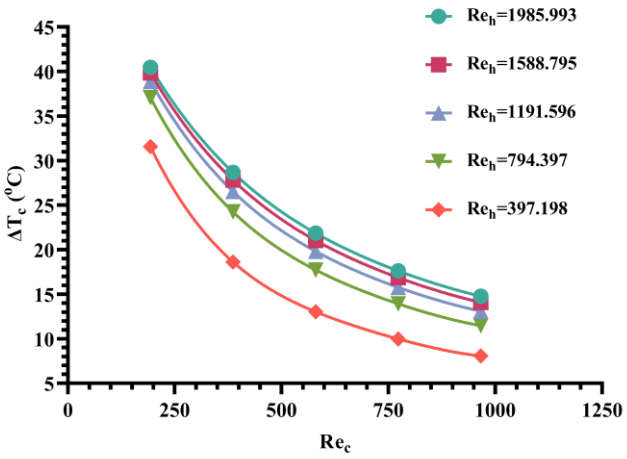

(b)

Fig. 8. Plot of ΔT_c vs Reynolds number of the cold fluid across a range of Reynolds numbers of hot fluid for (a) Snowflake-patterned PHE and (b)wishbone-patterned PHE

4.2 Effect of mass flow rate on effectiveness:

The mass flow rate is varied between 0.01kg/s and 0.05kg/s for both fluids, with an inlet temperature of 40^0C for cold fluid and 90^0C for hot fluid. The effectiveness (ε) of HX is given by Equation (10) to (12). The ε of heat exchanger is plotted against the mass flow rate of hot fluid as shown in Figure 9(a) and 9(b). It is observed that ε decreases as the mass flow rate of the hot fluid increases while keeping the mass flow rate of the cold fluid constant at 0.05 kg/s, but as the mass flow rate of cold fluid decreases to 0.04kg/s it can be seen that ε of heat exchanger increases as the mass flow rate of hot fluid increases. It can be seen that a similar trend is been followed as the mass flow rate of hot fluid is further decreased. Therefore, the performance of the heat exchanger is influenced by the fluid flow rate. When the hot fluid flows at a higher rate, its time inside the heat exchanger is shortened, leading to a decrease in effectiveness. If the mass flow rate of the cold fluid remains constant, altering the flow rate of the hot fluid may not affect the effectiveness. However, if the flow rate of the cold fluid is reduced, it enhances the effectiveness of the heat exchanger. This can be explained by Equation (13) and (14), the sudden increases in effectiveness of heat exchanger are due to its relation with Q_{max}, where Q_{max} is directly proportional to C_{min}.

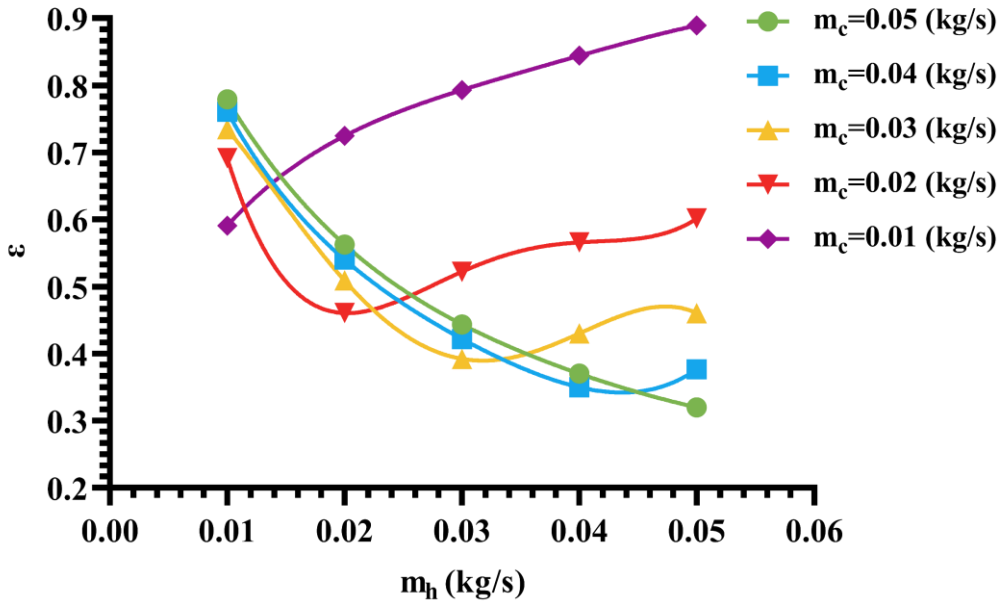

(a)

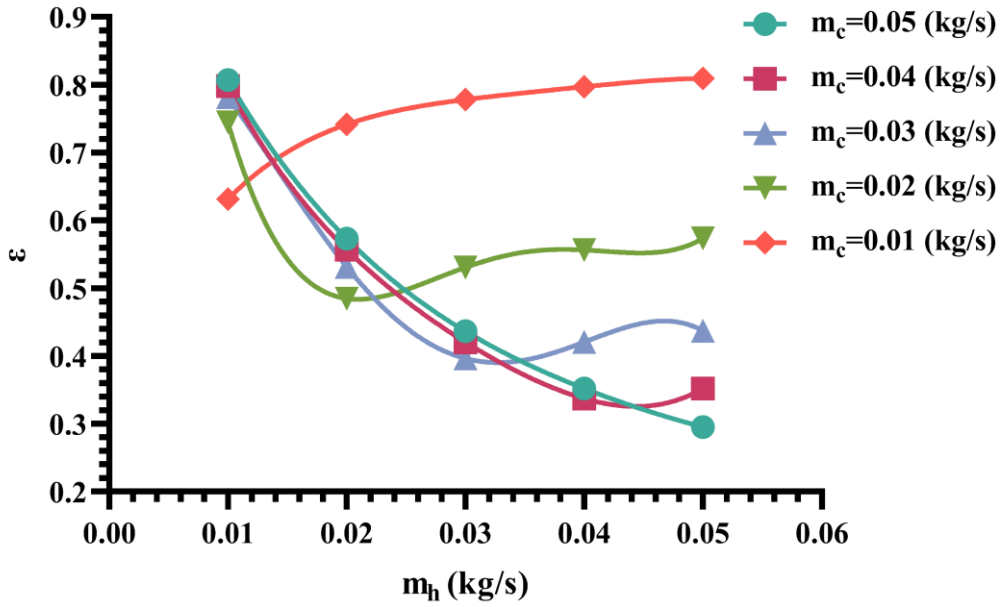

(b)

Fig. 9. Plot of ε vs m_h for varying m_c for (a) Snowflake-patterned PHE and (b)wishbone-patterned PHE

4.3 Effect of mass flow rate on Rate of Heat Transfer Q:

The mass flow rate is varied between 0.01kg/s and 0.05kg/s for both hot and cold fluid, with inlet temperatures of 90^0C for hot fluid and 40^0C for cold fluid. The heat transfer rate of is plotted against the mass flow rate of hot fluid as shown in Figure 10(a) and 10(b). It is observed that Q increases as the mass flow rate of hot fluid

increases, also Q increases with increasing the mass flow rate of cold fluid. It can be observed that Q is increased as the mass flow rate of cold fluid is varied between 0.01kg/s and 0.05kg/s. Increasing mass flow rates induce turbulence, thinning the thermal boundary layer. Despite a reduced temperature difference as explained in section 4.1, intensified convection enhances heat transfer rates, explaining the observed 35% to 80% increase in Q for snowflake-patterned PHE and 38% to 75% for wishbone-patterned PHE as cold fluid mass flow rate varies from 0.01 kg/s to 0.05 kg/s.

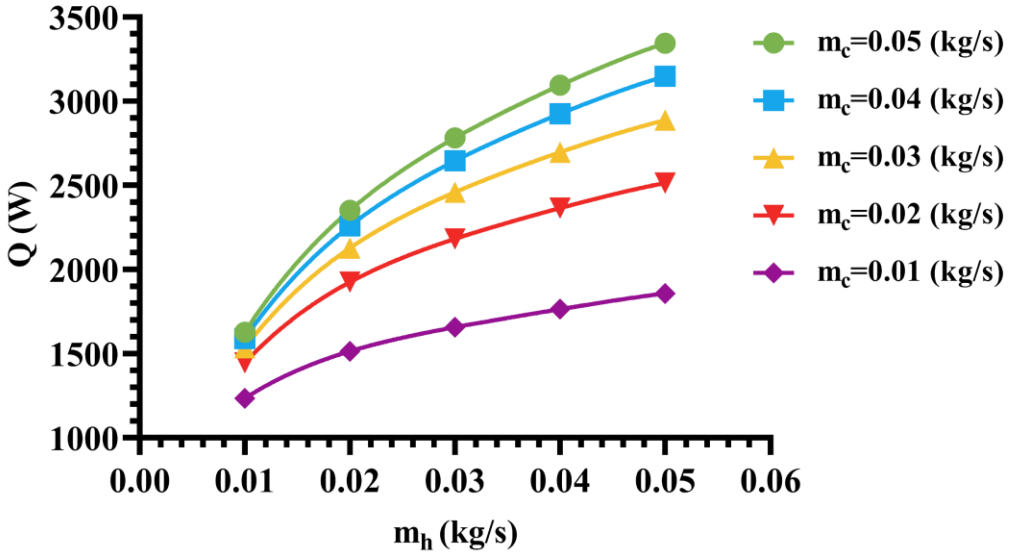

(a)

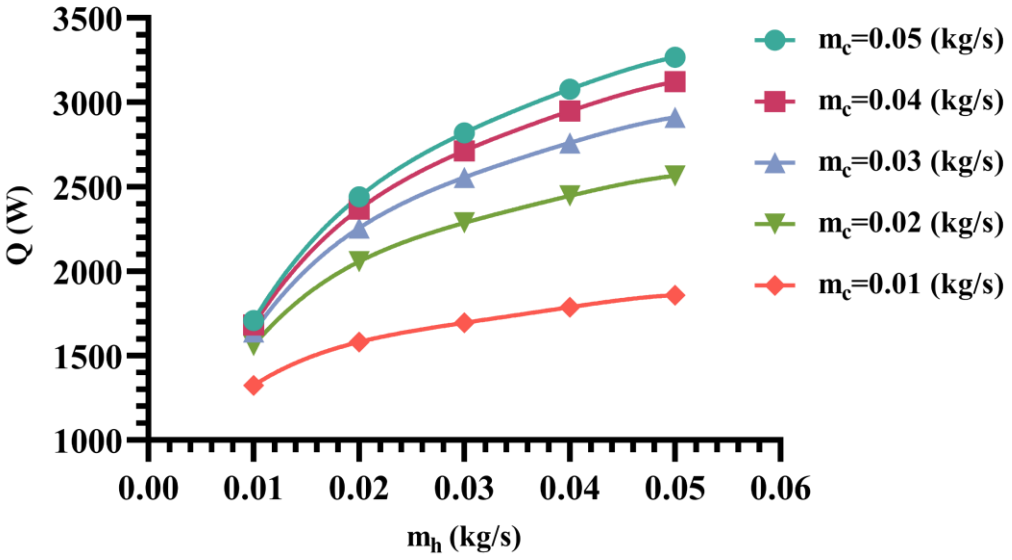

(b)

Fig. 10. Plot of Q vs m_h of the hot fluid across a range of m_c for for (a) Snowflake-patterned PHE and (b)wishbone-patterned PHE

4.5 Effect of snowflake and wishbone pattern on heat transfer coefficient along the surface of plate:

The HTC is obtained by using equation 15 and 16. The variation of HTC along the plate surface is shown in Figure 11(a) and 11(b). From the contours it can be observed that outside the patterned region, the local HTC is approximately 2000 (W/m^{2}K). However, along the patterns, the local HTC reaches approximately 9000 (W/m^{2}K). This indicates that the HTC is significantly higher in areas where the snowflake and wishbone patterns are present. The enhanced coefficient is attributed to the improved surface area and enhanced turbulence within these regions. Additionally, the average HTC is estimated to range between 5000 and 6000 (W/m2K).

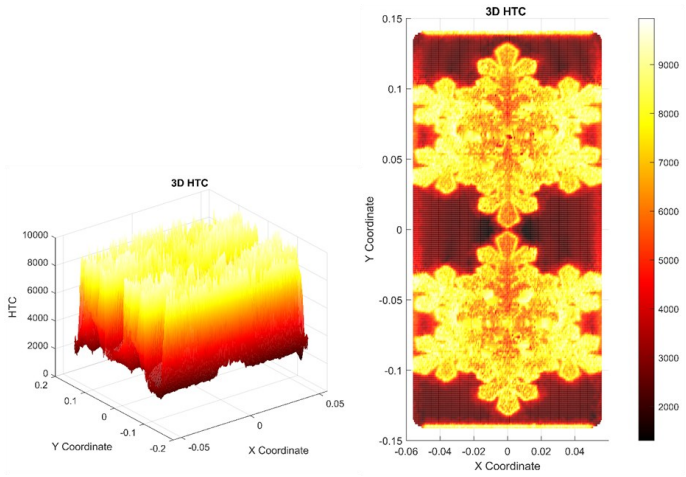

(a)

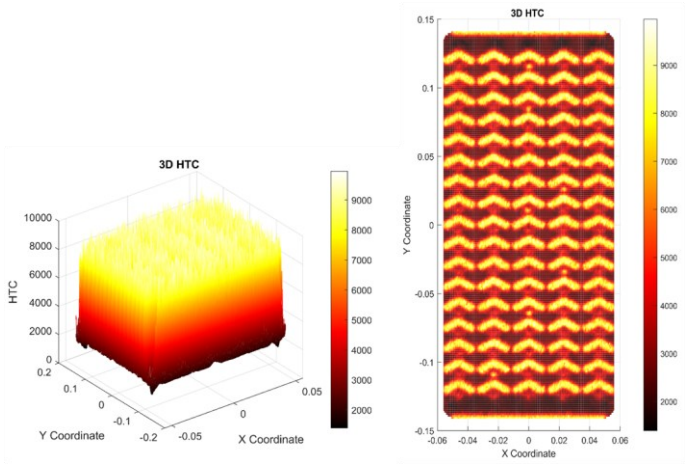

(b)

Fig. 11. Variation of HTC(W/m^{2}K) along the surface of plate for (a) Snowflake-patterned PHE and (b)wishbone-patterned PHE

4.6 Effect of corrugation pattern on pressure drop:

Pressure drop is an important parameter that has to be considered while designing a plate heat exchanger as pumping power is dependent on ΔP as given in Equation (18). The new designs have been compared with the experimental paper [2] as shown in Figure 12. It has been observed that the wishbone pattern has the minimum pressure drop when compared with the snowflake pattern and the chevron type. It is seen that drop in the pressure in snowflake pattern has been decreased by 36.9% when compared with chevron type and for wishbone pattern, it has been reduced by 80.88% for a flow rate of 0.078 kg/s.

$$Pumping\ Power = \Delta P * \dot{Q}$$
$$\dot{Q} = volume\ flow\ rate\ (m^3 / s) \tag{19}$$

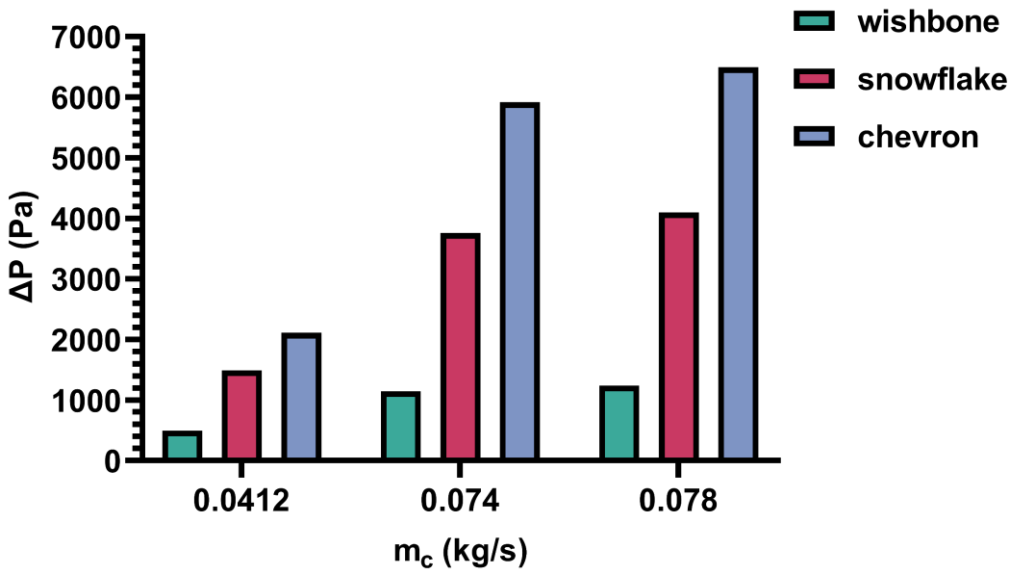

Fig. 12. Variation of ΔP for different mass flow rate

4.7 Effect of corrugation pattern on heat transfer rate Q:

The variation of heat transfer rate for different corrugation pattern has been shown in Figure 13. The heat transfer rate of the new design has been compared with the experimental paper [2]. It has been observed that the rate of heat transfer is maximum wishbone pattern when compared to the snowflake pattern and chevron pattern. The rate of heat transfer of snowflake pattern is improved by 22.5%, for wishbone pattern it is increased by 28.7% when compared with the chevron type for a flow rate of 0.0788 kg/s.

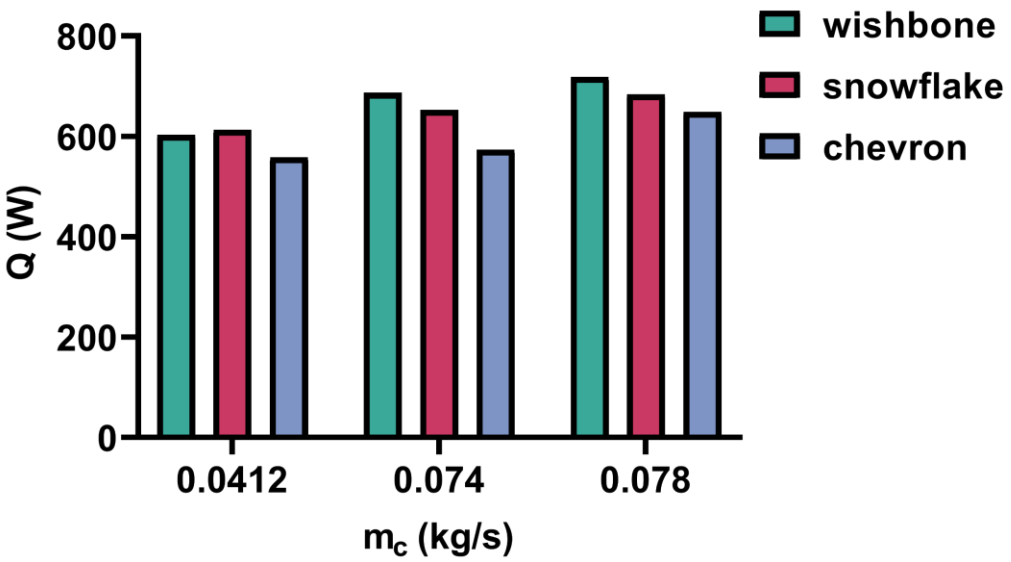

Fig. 13. Variation of heat transfer rate for various mass flow rate

4.8 Effect of corrugation pattern on HTC:

The variation of HTC with Reynolds for the snowflake and wishbone patterns has been shown in Figure 14. It has been observed that HTC increases as the Reynolds number increases for both snowflake pattern as well as wishbone pattern. It is seen that the snowflake pattern has 18% higher HTC value when compared with the wishbone pattern at Reynolds number of 1985.

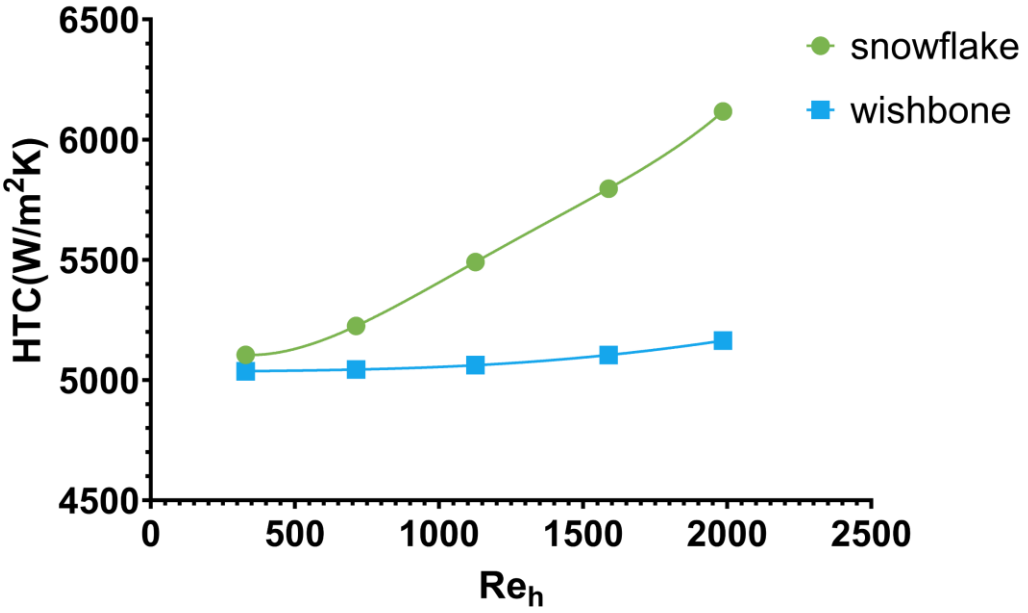

Fig.14. Plot of HTC vs Reynolds number

5.Conclusions

In the present study, snowflake and wishbone patterns are designed using a bionic approach and analyzed using ansys fluent with RNG k-ε as the turbulence model. To verify the methodology followed during analysis, CFD simulations are validated against experimental results investigated by Kwon et al. [2]. It was found that CFD results and experimental results had a mean deviation of 6.25%, indicating good numerical model accuracy. This suggests the model is suitable for further studies. Further analysis was performed on snowflake-patterned PHE and wishbone-patterned PHE for various mass flow rates. The effect of mass flow rate on effectiveness, pressure difference, HTC and, rate of heat transfer are summarized as follows:

1. The hot fluid ΔT_h decreases as its flow rate rises from 0.01kg/s to 0.05 kg/s in general. However, with respect to the proposed patterns, ΔT_h increases from 35% to 80% for snowflake pattern and 39% to 77% for wishbone pattern as mass flow rate of cold fluid rises from 0.01kg/s to 0.05kg/s. Further, a similar result can be seen for the cold fluid ΔT_c.

2. The effectiveness of PHE is found to depend on the mass flow rate of both fluids. The ε_{max} for snowflake-patterned PHE is 0.88 and that for wishbone-patterned PHE is 0.80 for a m_h=0.05kg/s and m_c=0.01kg/s.

3. The rate of heat transfer for hot fluid Q_h increases as the mass flow rate of hot fluid rises from 0.01kg/s to 0.05 kg/s in general for both the patterns. Whereas, it increases from 35% to 80% for snowflake-patterned PHE and 38% to 75% for wishbone-patterned PHE for the increase in m_c from 0.01kg/s to 0.05kg/s.

4. The HTC value is observed to be high near the snowflake and wishbone pattern compared to the remaining regions. Hence, high HTC enhances the overall heat transfer performance of PHE.

5. With regard to the drop in the fluid pressure, it is reduced to 36% for snowflake-patterned PHE and 80% for wishbone patterned PHE when compared with regular chevron patterned PHE [2].

6. HTC increases as Reynolds number increases for both snowflake-patterned PHE and wishbone-patterned PHE. The snowflake patterned PHE has 18% higher HTC value when compared with wishbone patterned PHE for a higher Reynolds number of 1985.

Reference

[1] Man Bae Kim and Chang Yong Park. An experimental study on single phase convection heat transfer and pressure drop in two brazed plate heat exchangers with different chevron shapes and hydraulic diameters. Springer Journal of Mechanical Science and Technology. Volume 31, pages 2559–2571.

[2] Oh Jin Kwon, Byung Hoon Shon, Yong Tae Kang. Experimental investigation on condensation heat transfer and pressure drop of a low GWP refrigerant R-1233zd(E) in a plate heat exchanger. Elsevier International Journal of Heat and Mass Transfer.

[3] Angela Mutumba, Francesco Coletti, Alex Reip, Mohamed M. Mahmoud & Tassos G. Karayiannis. Experiments and Correlations for Single-Phase Convective Heat Transfer in Brazed Plate Heat Exchangers. Taylor and Francis Heat Transfer Engineering, Volume 44.

[4] Divya P. Soman, S. Karthika, P. Kalaichelvi∗, T.K. Radhakrishnan. Experimental study of turbulent forced convection heat transfer and friction factor in dimpled plate heat exchanger. Elsevier Applied thermal Engineering , Volume 162.

[5] Divya P. Soman, S.Karthika, D.T. Valan, P. Kalaichelvi , T.K. Radhakrishnan .Computational Fluid Dynamics Modelling and Analysis of Heat Transfer in Multichannel Dimple Plate Heat Exchanger. Iranian Journal of Chemistry and Chemical Engineering, Volume 41, pages 2071-2086.

[6] Selin Aradag, Yasin Genc & Caner Turk. Comparative gasketed plate heat exchanger performance prediction with computations, experiments, correlations and artificial neural network estimations. Taylor and Francis, Engineering Applications of Computational Fluid Mechanics, Volume 11, pages 467-482.

[7] Woosung Yoon, Ji Hwan Jeong. Development of a numerical analysis model using a flow network for a plate heat exchanger with consideration of the flow distribution. Elsevier International Journal of Heat and Mass Transfer, Volume 112, pages 1-17.

[8] H. B. Luan, J. P. Kuang, Z. Cao, Z. Wu, W. Q. Tao & B. Sundén. CFD analysis of two types of welded plate heat exchangers. Taylor and Francis An International Journal of Computation and Methodology, Volume 71, Pages 250-269.

[9] Mohammad Pourhoseinian, Neda Asasian-Kolur, Seyedmehdi Sharifian. CFD investigation of heat and moisture recovery from air with membrane heat exchanger. Elsevier Applied thermal Engineering, Volume 191.

[10] Pan Xu , Jian Wen , Xin Zhao , Hongwei Hao , Yanzhong Li. Numerical investigation on serrated fin of sub-atmosphere plate-fin heat exchanger used in superfluid helium system. Elsevier Cryogenics, Volume 119.

[11] Hiroki Kobayashi, Kentaro Yaji, Shintaro Yamasaki, Kikuo Fujita. Freeform winglet design of fin-and-tube heat exchangers guided by topology optimization. Elsevier Applied thermal Engineering, Volume 161.

[12] Aoke Liu , Guanghui Wang , Dingbiao Wang , Honglin Yuan. Study on the thermal and hydraulic performance of fin-and-tube heat exchanger based on topology optimization. Elsevier Applied thermal Engineering, Volume 197.

[13] Hassene Djemel , Sirine Chtourou , Mounir Baccar. Three-dimensional numerical study of a new intercooler design. Elsevier International Journal of Thermofluids, Volume 17.

[14] Merve Göltaş , Barış Gürel , Ali Keçebaş , Volkan Ramazan Akkaya , Onur Vahip Güler, Karani Kurtuluş, Emine Yağız Gürbüz. Thermo-hydraulic performance improvement with nanofluids of a fish-gill-inspired plate heat exchanger. Elsevier Energy, Volume 253.

[15] Barı ş Gürel, Volkan Ramazan Akkaya, Merve Göltaş, Çağla Nur Şen, Onur Vahip Güler, Mehmet İlkay Koşar, Ali Keçebaş. Investigation on flow and heat transfer of compact brazed plate heat exchanger with lung pattern. Elsevier Applied Thermal Engineering.

[16] Radia Eldeeb, Vikrant Aute, Reinhard Radermacher. Pillow plate heat exchanger weld shape optimization using approximation and parallel parameterized CFD and non-uniform rational B-splines. Elsevier International Journal of Refrigeration, Volume 110, pages 121-131.

[17] Yongxue Zhan, Bohui Lu, Zixi Wang, Jianjun Zhu, Jinya Zhang , Cong Wang. Experimental investigation on the charging and discharging performance enhancement of a vertical latent heat thermal energy storage unit via snowflake fin design. Elsevier International Journal of Heat and Mass Transfer.

[18] Ansys Fluent 12.0 user guide